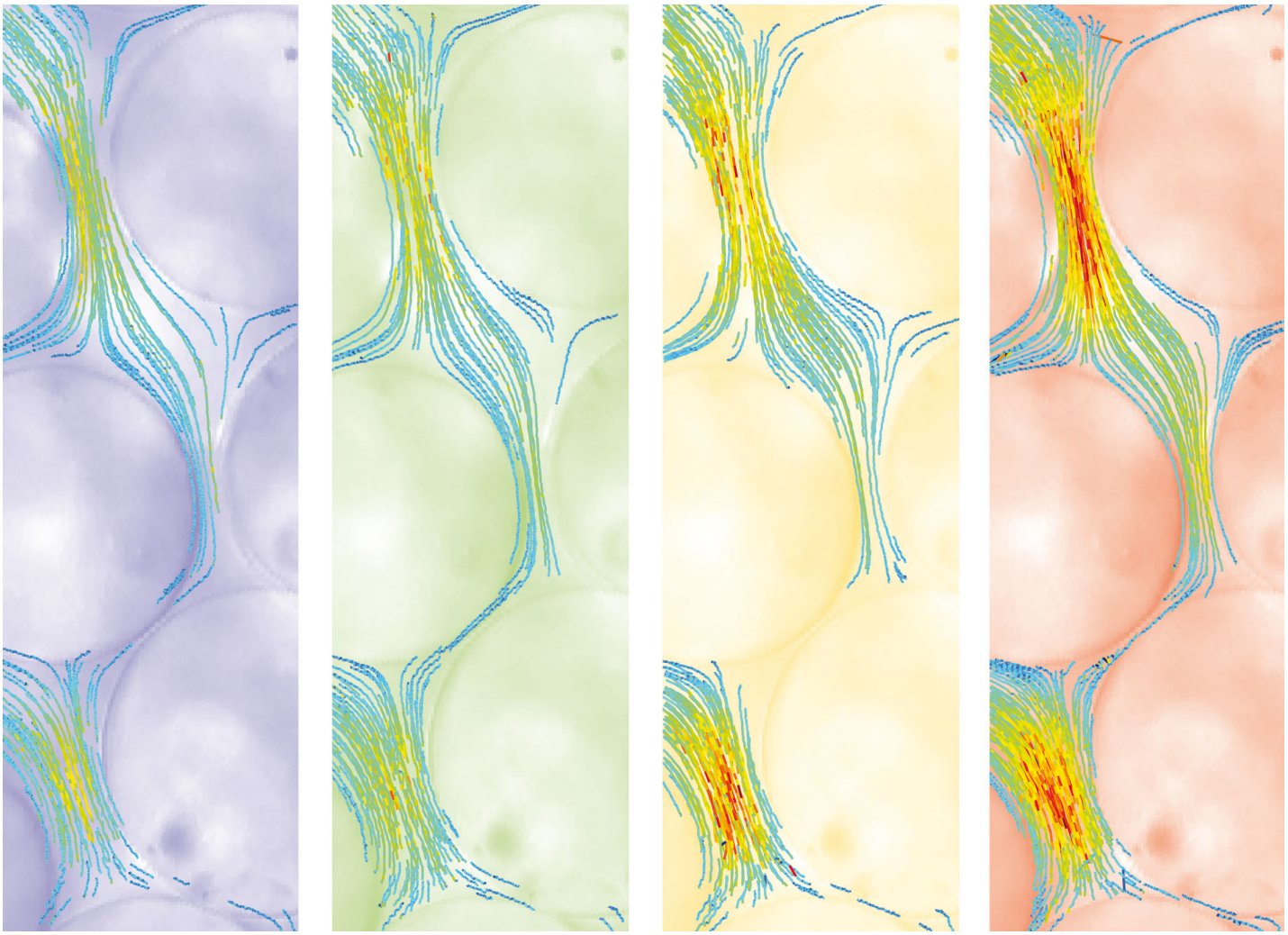

Highlighting research from Jacinta Conrad and Ramanan Krishnamoorti in Chemical and Biomolecular Engineering at the University of Houston.

Nanoparticle dispersion in disordered porous media with and without polymer additives

The long-time transport coefficients of particles flowed through disordered porous media in water, in a viscous Newtonian fluid, and in a non-Newtonian shear-thinning polymer solution collapse onto scaling curves, indicating that addition of polymer does not impact the particle dispersion.

As featured in:

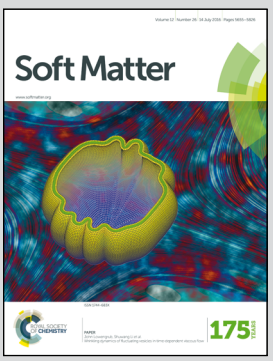

See Ramanan Krishnamoorti, Jacinta C. Conrad *et al.*, *Soft Matter*, 2016, **12**, 5676.

ROYAL SOCIETY OF CHEMISTRY

www.softmatter.org

Registered charity number: 207890

Soft Matter

PAPER

View Article Online
View Journal | View Issue

Cite this: *Soft Matter*, 2016, 12, 5676

Nanoparticle dispersion in disordered porous media with and without polymer additives†

Firoozeh Babayekhorasani,[a] Dave E. Dunstan,[b] Ramanan Krishnamoorti*[ac] and Jacinta C. Conrad*[a]

Received 26th February 2016,
Accepted 22nd May 2016

DOI: 10.1039/c6sm00502k

www.rsc.org/softmatter

In purely viscous Newtonian fluids, mechanical mixing of the fluid stream as it moves through an unstructured porous medium controls the long-time dispersion of molecular tracers. In applications ranging from environmental remediation to materials processing, however, particles are transported through porous media in polymer solutions and melts, for which the fluid properties depend on the shear rate and extent of deformation. How the flow characteristics of polymer solutions affect the spreading of finite-sized particles remains poorly understood – both on the microscopic scale as local velocity profiles, and on the macroscale as dispersion. Here, we show across a range of flow rates and disordered porous media configurations that the long-time transport coefficients of particles flowed in water, in a viscous Newtonian fluid, and in a non-Newtonian shear-thinning polymer solution collapse onto scaling curves, independent of the fluid rheology. Thus the addition of polymer does not impact nanoparticle dispersion through disordered porous media.

Introduction

Control over transport of nanoparticles in polymer solutions flowed through highly confined porous media is required to deliver drugs and diagnostics,[1,2] to safely produce hydrocarbons,[3] and to process polymer nanocomposites.[4,5] In purely viscous Newtonian fluids, the long-time spreading of particles flowed at high shear rates through a porous medium is controlled by mechanical mixing of the fluid stream.[6,7] By contrast, the effects of viscoelasticity arising from the presence of polymers at high concentrations on particle spreading in confined flows of non-Newtonian fluids[8–14] through either microscopic particle flow profiles or macroscale particle transport measures remains poorly understood.

In Newtonian fluids flowed through a disordered porous medium, molecular diffusive processes control the long-time (asymptotic) dispersion of molecular tracers[6,7] in both the axial and transverse directions when advection is weak compared to diffusion; similarly, advective processes due to the stochastic velocity field coupled to diffusion control dispersion in the opposite limit, when diffusion is weak compared to advection.[6,7] The disordered structure of the medium generates uniform mixing, enabling the tracers to sample all positions within the bed.[6] The pore-scale velocity profiles reflect the spatial heterogeneity of the medium[15] but do not affect long-time dispersion in the mechanically-mixed regime.[16] The importance of uniform mixing is emphasized through comparisons to geometrically ordered (periodic) porous media, in which particles can exhibit deterministic trajectories[17,18] and local coupling between diffusive and advective transport on short time and length scales alters dispersion.[19]

In non-Newtonian fluids, such as semi-dilute and concentrated polymer solutions, additional mechanisms that may affect particle dispersion arise from the interplay of the fluid rheology and spatial confinement within a disordered (non-periodic) pore network that does not exhibit long-range order. The converging–diverging pore structure imposes deformations that typically include both shear and elongational components, thus generating complex flows.[20] When the rate of shear-imposed deformation $\dot{\gamma}$ is less than the characteristic relaxation rate $1/\lambda$ of the fluid, as quantified by the Weissenberg number $\mathrm{Wi} = \lambda\dot{\gamma} < 1$, Darcy's law can be used with the time-dependent effective viscosity of the non-Newtonian fluid. At higher shear rates, however, the pressure gradient does not necessarily change linearly with the flow velocity and contrasting effects are reported for the flow characteristics of non-Newtonian fluids. In several studies, non-Newtonian flow through a narrow channel generates novel phenomena. As one example, the velocity profile of a non-Newtonian power-law fluid flowing through a straight channel exhibits deviations

[a] *Chemical and Biomolecular Engineering, University of Houston, Houston, Texas 77204, USA. E-mail: ramanan@uh.edu, jcconrad@uh.edu*
[b] *Chemical and Biomolecular Engineering, University of Melbourne, 3010, Australia*
[c] *Department of Chemistry, University of Houston, Houston, Texas 77204, USA*

† Electronic supplementary information (ESI) available: (1) Detailed description of the bed characterization (Fig. S1); (2) a description of how the dimensionless numbers for this study were calculated (Tables S1–S8); and (3) supplementary results for other packed bed configurations, other flow rates, and for water solutions (Fig. S2–S17). See DOI: 10.1039/c6sm00502k

from the Poiseuille equation that depend on the power law exponent.[21] Furthermore, nonlinearities arising in the flow of viscoelastic fluids through very narrow channels can manifest as elastic instabilities, such as those seen near cylinders confined within a microchannel.[8] These fluid instabilities typically couple with the microscale confinement experienced by the viscoelastic fluid to enhance both velocity and stress fluctuations, which in turn are proposed to generate, *e.g.*, elastic turbulence.[12–14] Conversely, when the channel or pore size is sufficiently small, flow through a porous medium can break the non-Newtonian characteristics of yield stress or shear thinning fluids.[22,23] In this scenario the deformation imposed by the pore network effectively averages out the non-Newtonian properties of the fluid. Which of these effects governs the dispersion of particles that are suspended in shear-thinning polymer fluids and flowed through disordered porous media is not known.

Using as a model porous medium disordered (non-periodic) packed beds of sintered micron-sized glass spheres, here we show across a range of flow rates and pore configurations that the long-time longitudinal and transverse dispersion coefficients of particles flowed in water, in a mixture of glycerol and water, and in a shear-thinning semidilute solution of partially hydrolyzed polyacrylamide collapse onto scaling curves, independent of the fluid rheology. This result contrasts to previous studies in periodic ordered media, where the non-Newtonian characteristics of a semidilute polyacrylamide solution dramatically enhanced the transverse dispersion.[14] Our study suggests that the rheology of semidilute and concentrated polymer shear-thinning solutions alone cannot be used to control spreading of particles. Instead, solution rheology must be coupled to regular periodic (geometric) order within the porous medium to modulate the particle dispersion.

Results and discussion

To determine the effect of macromolecular additives on the transport of nanoparticles in highly confined and disordered (non-periodic) media, we formulated two solutions: a Newtonian 90/10 w/w mixture of glycerol and water, and a non-Newtonian solution of aqueous 0.1 wt% partially hydrolyzed polyacrylamide (HPAM) of weight-averaged molecular weight M_w = 8 000 000. Using the overlap concentration of the polymer c^* = 0.016 wt%, the normalized polymer concentration is c/c^* = 6.25, so that that the HPAM solution is semidilute but not entangled.[24] The HPAM solution is viscoelastic (Fig. 1): the frequency-dependent elastic and viscous moduli are of similar order of magnitude, and the solution exhibits strong shear-thinning. Its viscosity at zero shear rate [2.7 Pa s^{-1}] is an order of magnitude larger than that of the glycerol–water mixture [0.11 Pa s^{-1}]; at a shear rate of $\dot{\gamma} \approx 1.6\ s^{-1}$, however, its viscosity equals that of the glycerol–water mixture.[25] The linear dynamic oscillatory rheology (viscous and elastic moduli as a function of frequency) and the steady shear rheology (viscosity as a function of shear rate) obey an empirical Cox–Merz rule (Fig. 1(b), inset).[26] Fluorescent polystyrene nanoparticles were added to both solutions at a concentration of 2×10^{-3} wt% and tumbled on a roll mill for up to 24 hours to ensure that the particles were uniformly dispersed.

Borosilicate microcapillary cells of inner side length 0.7 mm and length of 5 cm were packed with one of three different sizes of beads: borosilicate glass microspheres of diameter 5.4 ± 0.3 μm or 10.0 ± 1.0 μm or soda lime glass microspheres of diameter 30.1 ± 1.1 μm. After sintering, the average porosity ϕ, average pore size d_{pore}, and average confinement length l_c of the beds were characterized using two-dimensional confocal microscopy. Particles suspended in HPAM solutions, in glycerol–water, and in deionized water were flowed through the beds, imaged with high-speed confocal microscopy at 110 frames per s, and tracked over time using standard algorithms.[27] By varying the flow rate from 5 to 20 μl h^{-1} (accessing in different fluids Péclet numbers of $2 \times 10^1 < Pe < 3 \times 10^5$), we accessed flows in the coupled diffusion–advection ($6 < Pe < 72$) and mechanically-mixed ($Pe > 72$) regimes.[7]

For a given fluid, the microscopic flow profiles do not depend on the bed geometry (Fig. 2 and Fig. S3–S5, ESI†). At a fixed bulk flow rate, the longitudinal (x) and transverse (y) distributions of velocity for nanoparticles flowing through beds of varying bead

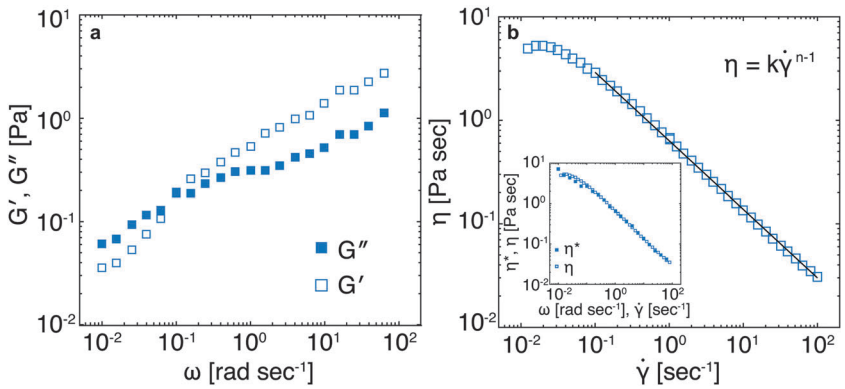

Fig. 1 Rheology of the HPAM solution. (a) Linear dynamic oscillatory shear-based elastic (G') and viscous (G'') moduli as a function of the angular frequency ω. (b) Viscosity η as a function of the steady shear rate $\dot{\gamma}$. The line indicates a fit to the power-law (shear-thinning) function shown. Inset to (b): The complex viscosity η^* (as a function of angular frequency ω) and the viscosity η (as a function of the steady shear rate $\dot{\gamma}$) obey an empirical Cox–Merz rule.[26]

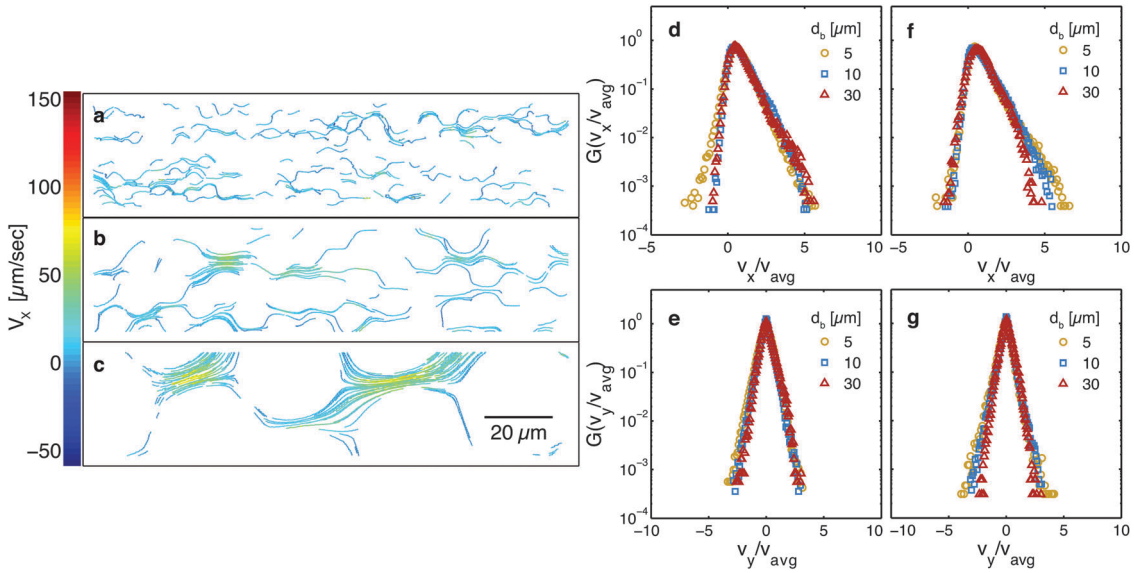

Fig. 2 Dependence of normalized velocity distributions on pore size for glycerol/water and for polymer solutions. (a–c) Trajectories of nanoparticles transported through porous beds with bead diameter (d_b) of (a) 5 μm, (b) 10 μm, or (c) 30 μm at an inlet flow rate of 5 μl h^{-1}. Colors indicate the velocity along the flow direction (v_x). (d–g) Normalized distributions of longitudinal [$G(v_x/v_{avg})$, d and f] and transverse [$G(v_y/v_{avg})$, e and g] velocities for nanoparticles transported in (d and e) a glycerol/water mixture (90 w/w%) and (f and g) an HPAM solution (0.1 w/w%; $c/c^* \sim 6.25$) at inlet flow rate of 5 μl h^{-1} through a porous bed with bead diameter of 5 μm (gold circle), 10 μm (blue square), or 30 μm (red triangle). The bead diameter and pore size do not affect the normalized distributions of nanoparticle velocities for glycerol/water or for polymer fluids.

size collapse onto scaling curves after normalizing by the average bulk flow velocity v_{avg}. Distinct curves are obtained for glycerol/water (Fig. 2d and e) and for polymer (Fig. 2f and g) solutions. In both types of fluids the longitudinal velocity distributions $G(v_x/v_{avg})$ have exponentially-stretched positive tails, consistent with earlier measurements of non-Gaussian velocity distributions from simulation[28] and experiment.[15,29] In both types of fluids the transverse velocity distributions $G(v_y/v_{avg})$ are non-Gaussian yet symmetric about zero, indicating that particle mobility does not have a preferred direction perpendicular to the bulk flow.

Similarly, the microscopic velocity distributions for the glycerol/water and for the polymer solutions are independent

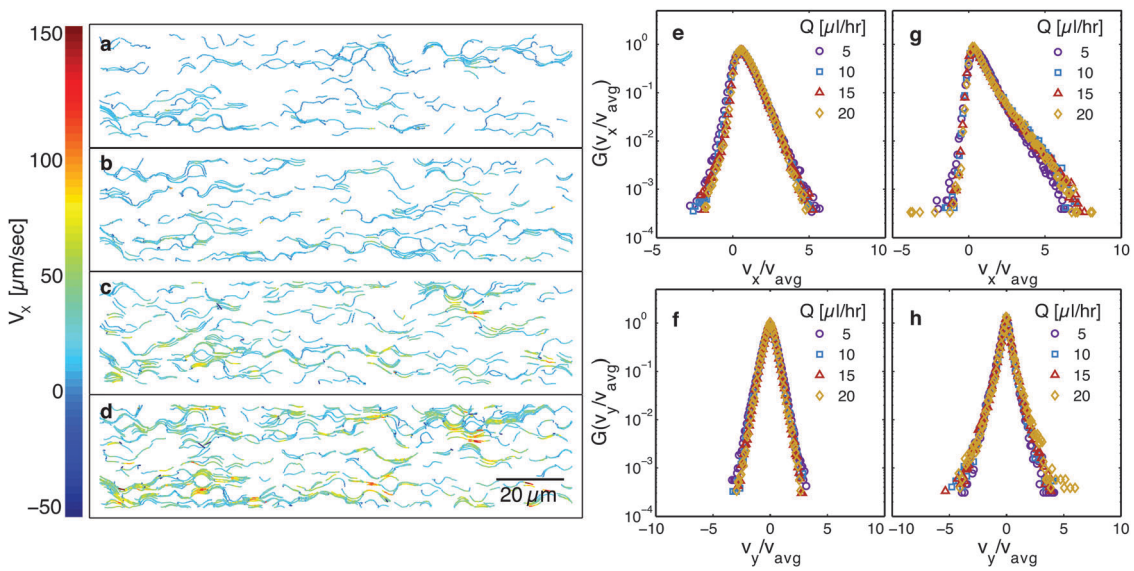

Fig. 3 Dependence of normalized velocity distributions on flow rate for glycerol/water and for polymer solutions. (a–d) Trajectories of nanoparticles transported through porous beds with bead diameter of 5 μm at bulk flow rates of (a) 5, (b) 10, (c) 15, and (d) 20 μl h^{-1}. Colors represent velocity variation along the flow direction (v_x). (e–h) Normalized distributions of longitudinal [$G(v_x/v_{avg})$, e and g] and transverse [$G(v_y/v_{avg})$, f and h] velocities for nanoparticles in (e and f) a glycerol/water mixture (90 w/w%) and (g and h) an HPAM solution (0.1 w/w%; $c/c^* \sim 6.25$) at an inlet flow rate of 5 (purple circle), 10 (blue square), 15 (red triangle), or 20 (gold diamond) μl h^{-1} through a porous bed with bead diameter of 5 μm. The inlet flow rate does not affect the normalized distributions of nanoparticle velocities for glycerol/water or for the polymer fluid.

of the bulk flow rate for a fixed bead size (Fig. 3 and Fig. S6 and S7 in the ESI†). The scaling curves for the Newtonian glycerol/water mixture and the non-Newtonian HPAM solution can be superimposed for modest normalized velocities but diverge for larger velocities (Fig. S9 in the ESI†), which appear more frequently in the HPAM solutions. The increase in velocity likely arises from coupling of the particle motion to segmental dynamics in the polymer on short time scales.[30]

To connect the microscopic velocity distributions to macroscopic dispersion, we calculate the time-dependent longitudinal dispersion coefficients[31] as $D_L(t) = \frac{1}{2}\frac{d\sigma_L^2}{dt} = \int C_L(t')dt'$, where $C_L(t)$ is the autocovariance of the nanoparticle velocity $v_x(t)$ along the flow direction (x), given by $C_L(t) = \sum_{i=1}^{N}\left(v_{x,i}(t) - \langle v_x\rangle\right)\left(v_{x,i}(0) - \langle v_x\rangle\right)$, and $\sigma_L^2(t)$ is the second moment of the longitudinal particle displacements. The time-dependent transverse dispersion coefficient $D_T(t)$ is similarly defined. We normalize $D_L(t)$ and $D_T(t)$ by the quiescent diffusivity of the nanoparticles measured in the appropriate matrix fluid and porous medium, D_q, and the lag time by the characteristic convective time scale, d_b/v_{avg}. On short time scales, both D_L/D_q and D_T/D_q increase with dimensionless time $\tau = tv_{avg}/d_b$ as the particles are advected and mixed by the flow in the porous medium (Fig. 4), consistent with the idea that the pore-scale velocity affects the local flow behavior.[16]

Both ratios initially increase as power laws with τ. On long time scales, D_L/D_q and D_T/D_q are expected to approach an asymptotic limiting value if the time domain of the correlation is smaller than the residence time in the porous medium. For longitudinal dispersion this time scale is set by convection and is typically $5 < \tau < 10$ [ref. 31 and 32]. The time corresponding to maximum longitudinal dispersion decreases approximately linearly with increasing bead diameter (Fig. S10 and S11 in the ESI†). Transverse dispersion approaches a local maximum at a normalized time of $\tau \approx 0.4$ and decreases slightly on longer time scales, approximately independent of the flow rate and bead diameter (Fig. S10 and S11 in the ESI†); the slight decrease on longer times reflects contributions from the slowest particles in strong confinement.[33] The timescale is in reasonable agreement with the asymptotic prediction,[6] $\tau > \sqrt{1-\varphi} \approx 0.8$, calculated using the average bed porosity $\varphi \approx 0.35$ for different beds. The different time-dependence of the longitudinal and transverse dispersion coefficients arises from that of the velocity autocovariances: the transverse autocovariance is negative over an intermediate time range, for beds composed of 5 μm and 10 μm beads, whereas the longitudinal autocovariance is strictly positive for all beds (Fig. S13–S15 in the ESI†). Physically, one explanation for this difference is that a finite fraction of particles that move around a bead particle gradually reduce their transverse displacement after an initial increase

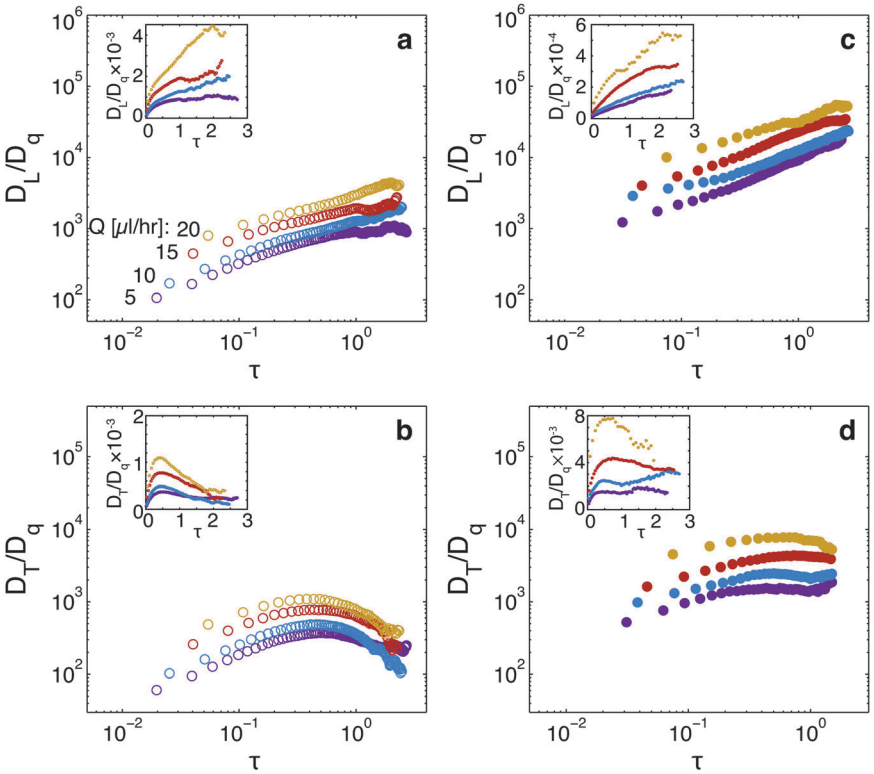

Fig. 4 Time dependent dispersion of nanoparticles in glycerol/water and polymer solutions. Normalized longitudinal (D_L/D_q, a and c) and transverse (D_T/D_q, b and d) dispersion coefficients of nanoparticles in (a and b) a glycerol/water mixture (90 w/w%) and (c and d) an HPAM solution (0.1 w/w%; $c/c^* \sim 6.25$) as a function of normalized lag time ($\tau = tv_{avg}/d_b$) through a porous bed with bead diameter of 5 μm. Colors indicate different flow rates: 5 μl h^{-1} (purple), 10 μl h^{-1} (blue), and 15 μl h^{-1} (red), and 20 μl h^{-1} (gold). Open symbols indicate the glycerol/water solution and closed symbols indicate the HPAM polymer solutions. The insets in each panel show the same data on linear axes.

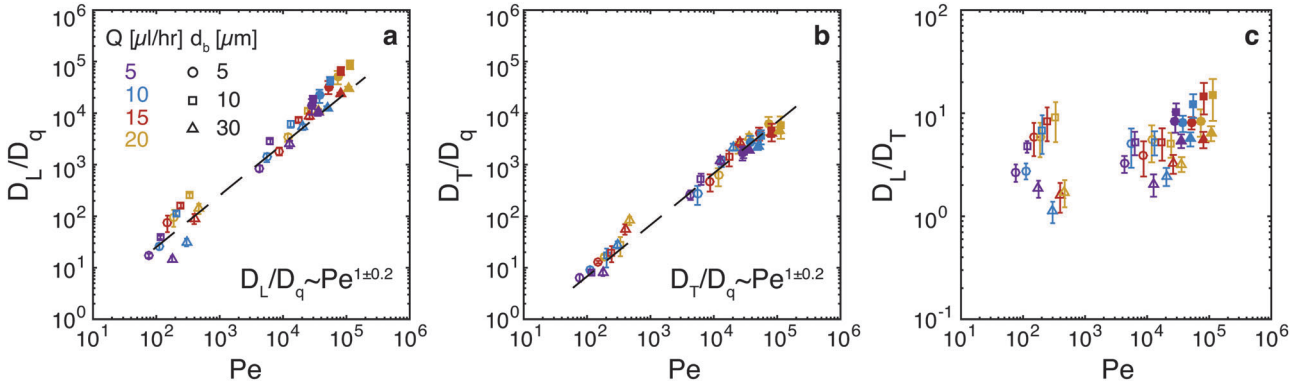

Fig. 5 Scaling collapses for asymptotic longitudinal and transverse dispersion coefficients. (a) Normalized longitudinal dispersion coefficient (D_L/D_q) and (b) normalized transverse dispersion coefficient (D_T/D_q) of nanoparticles in water, in a glycerol/water mixture (90 w/w%), or in HPAM solution (0.1 w/w%; $c/c^* \sim 6.25$) as a function of Péclet number Pe = $v_{avg}l_c/D_q$, where the characteristic length scale is taken as the average confinement length l_c. Dashed line indicates a linear fit. (c) Ratio of longitudinal and transverse dispersions (D_L/D_T) as a function of Pe. Colors indicate the flow rate: (purple) 5, (blue) 10, (red) 15, or (gold) 20 μl h^{-1}. Symbols indicate the bead diameter: (circle) 5 μm, (square) 10 μm, or (triangle) 30 μm. Open symbols indicate Newtonian fluids (glycerol/water mixture or water) and closed symbols indicate the non-Newtonian polymer solution (HPAM). Error bars indicate the propagated errors from the calculated values of D_L and/or D_T.

(following streamlines around the sphere surface), generating a negative autocovariance on intermediate time scales;[31] by contrast, the vast majority of particles are convected in the (positive) flow direction, so that the longitudinal autocovariance remains positive.

From the limiting values of the dispersion ratios, we extract the long-time asymptotic dispersion coefficients. Across the range of bed particle diameters and flow rates accessed here, the normalized longitudinal and transverse dispersion coefficients collapse onto master curves (Fig. 5) as a function of the Péclet number Pe = $v_{avg}l_c/D_q$ (Tables S6–S8 in the ESI†). The scaling collapse across different bead diameters and flow rates for a given fluid supports the microscopic definitions of D_L, D_T, and Pe employed here. The scaling collapse across the different fluids indicates that the viscoelastic characteristics of the

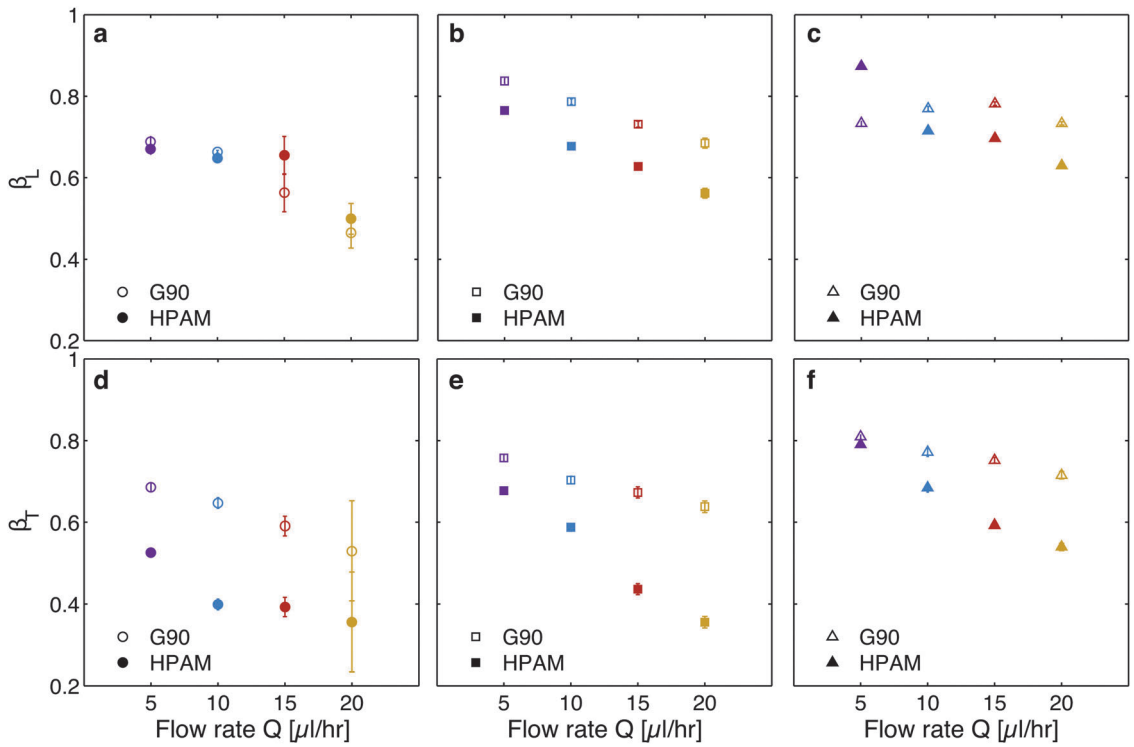

Fig. 6 Short-time dispersion exponents in glycerol/water and in polymer solutions. Power-law exponent of time-dependent longitudinal β_L (a–c) and transverse β_T (d–f) dispersion coefficients in porous beds with bead diameter of (a and d) 5 μm, (b and e) 10 μm, and (c and f) 30 μm. Open symbols indicate the Newtonian 90/10 glycerol/water mixture (G90) and closed symbols indicate the non-Newtonian polymer solutions (HPAM). Error bars indicate errors associated with the fitting values for each parameter.

polymer solution do not affect the dispersion of nanoparticles flowed through disordered media. We posit that the non-periodic structure of the packed bed effectively averages out any enhanced fluctuations arising from the polymer fluid viscoelasticity; indeed, the transverse mean-square displacements are strictly increasing (Fig. S16 in the ESI†), in contrast to the oscillations reported for particles in spatially periodic media in ref. 14. Both D_L/D_q and D_T/D_q scale linearly with Pe, consistent with earlier results across a similar range of Pe in random porous media. The ratio of the longitudinal and transverse dispersion coefficients D_L/D_T varies between 1 and 10. For the largest bead size ($d_b \approx 30$ μm) D_L/D_T is approximately unity, showing that the particles uniformly disperse in all directions. As the bed particle diameter is decreased D_L/D_T increases slightly, consistent with preferential transport along the longitudinal direction enhanced by confinement.[19]

The addition of the polymer does not affect asymptotic dispersion in the mechanically-mixed regime (after compensating for the increased viscosity). On shorter time scales, however, differences in the approach to asymptotic dispersion arise from differences in the shear-rate-dependent fluid response. We fit power-laws to the short-time limit in Fig. 4 (*i.e.* $D_L \sim \tau^{\beta_L}$ and $D_T \sim \tau^{\beta_T}$) and extract the scaling exponents β_L and β_T. The flow-rate dependence and the magnitude of β_L is similar for glycerol–water and HPAM solutions, consistent with the idea that the evolution of longitudinal dispersion is related to the total distance traveled through the packed bed (Fig. 6a–c).[16] Similarly, the flow-rate dependence of the transverse exponent β_T for glycerol–water is similar across all bed configurations (open symbols in Fig. 6d–f). By contrast, the dependence of β_T on flow rate becomes weaker as Wi is increased (*e.g.* as l_c is decreased) in the HPAM solutions (closed symbols in Fig. 6d–f). The differences in the scaling exponents (and hence in the time to reach asymptotic dispersion) may reflect coupling between the dynamics of the particles and polymer chains on short time scales,[25] where advection is coupled to diffusive mixing.[7] Nonetheless, random mixing in the disordered porous medium ensures that the viscoelastic characteristics of the polymer solution do not affect the asymptotic dispersion coefficients. This finding is in contrast to results reported for periodically-ordered porous media, in which elastic effects in a viscoelastic fluid enhance transverse dispersion.[14] In that case, velocity fluctuations enhanced by the fluid elasticity couple to the deterministic lateral displacements[17,18] arising from the periodic post structure.

Conclusions

We show that the long-time dispersion of particles suspended in a viscous mixture of glycerol and water or in a viscoelastic polymer solution and flowed through a disordered porous medium is identical, independent of the fluid rheology. Dispersion of particles suspended in polymer solutions in disordered porous media hence contrasts sharply to that observed in structured media. In semi-dilute polyacrylamide solutions, for example, elastic turbulence enhances velocity fluctuations.[34] In structured media (with geometrically ordered obstacles) this process promotes streamline crossing and dramatically enhances transverse particle dispersion,[14] because the fluctuations are not averaged out by the geometry of the medium. Indeed, the transverse dispersion coefficient D_T as a function of the Weissenberg number [Fig. S17 in the ESI†] increases by less than an order of magnitude across the Wi range probed in these experiments; this is in contrast to the two-order of magnitude increase across a similar range of Wi reported for periodic porous media.[14] This comparison highlights the critical role of the random mixing provided by disordered porous media in suppressing enhanced velocity fluctuations that arise due to the non-Newtonian solution rheology. We expect that other changes in suspension properties that enhance variations in velocity, such as increasing the concentration of particles,[35] may similarly increase dispersion.

The insensitivity of particle dispersion to the polymer solution rheology affects the choice of fluids used in applications demanding control over particle structure, dispersion, and transport. In applications involving disordered porous media, such as chromatographic separations[36,37] or hydrocarbon extraction *via* enhanced oil recovery,[3] existing models for asymptotic dispersion in Newtonian fluids can be applied as-is to predict and control particle transport. For these disordered media, changing the fluid characteristics alone (without modifying the pore arrangement and distribution) will not modify particle dispersion. Instead, fundamentally different strategies are required to increase dispersion in applications for which particles must be uniformly dispersed, as in 3-D printing of particle-laden polymer resins[38] or in processing of polymer nanocomposites.[39] Here particles suspended in polymer solutions and/or melts must be transported through an ordered pore or channel structured nozzles to ensure uniform dispersion. Hence we expect that modulating the flow geometry, not the fluid rheology, is the most promising route to tailor dispersion.

Materials and methods

Preparation of nanoparticle-solution dispersions

Fluoro-Max dyed red aqueous fluorescent polystyrene nanoparticles of diameter $d_{NP} = 400$ nm at concentration of 1 wt% were purchased from Thermo Fisher Scientific. Hydrolyzed polyacrylamide (HPAM) polymer of weight-averaged molecular weight (M_w) of 8 000 000 Da (FLOPAAM 3330) was provided by SNF. The degree of hydrolysis was 25–30% as reported by the manufacturer. We prepared an aqueous solution of HPAM in deionized water with concentration of $c_{HPAM} = 0.1$ wt%. We also prepared a glycerol/water mixture at concentration 90 wt% of glycerol (G90). Polystyrene nanoparticles were added to the HPAM solution, to the G90 solution, and to deionized water at concentration of 2×10^{-3} wt%. The nanoparticle-solution dispersions were then tumbled on a roll mill for 6–24 hours to ensure that all dispersions were fully homogenized.

Fabrication of porous media

Borosilicate capillary cells with square cross-section, inner side length of 0.7 mm, wall thickness of 0.14 mm, and length of 5 cm were purchased from VitroCom. Borosilicate glass microspheres

with diameter of 5.4 ± 0.3 μm and 10.0 ± 1.0 μm and soda lime glass microspheres with diameter of 30.1 ± 1.1 μm were purchased from Thermo-Scientific. The square capillary was filled with monodispersed glass particles to generate a 3D porous medium of length 5 mm. The glass particles were slightly sintered to remain stationary in the channel. Both ends of the square capillary were attached to PTFE tubing with inner diameter of 1 mm. A syringe pump working at constant displacement was connected to the tubing to feed the capillary.

Imaging of nanoparticles through porous media

Samples were imaged using a SP8 Leica inverted confocal microscope equipped with a 40× immersion oil lens with numerical aperture (NA) of 1.30. We acquired 6000 frames at 110 frames per second (fps) with a pixel size of 0.284 μm and image size of 145.31 × 36.11 μm^2. We took multiple movies of each sample at nine different x–y locations within the bed, but constant z position, at each of four flow rates (Q = 5, 10, 15, and 20 μl h^{-1}). The x–y locations were kept constant at the different flow rates.

Tracking of nanoparticles through porous media

A single particle tracking algorithm[27] was applied to locate and track nanoparticles over time. Particle trajectories were then used to calculate the velocity of nanoparticles along and transverse to the flow direction.

Characterization of pore and throat size of porous media

To visualize the bed structure, we suspended Rhodamine-B solution (Wako Pure Chemical Industries, Ltd) in a mixture of carbon disulfide (index of refraction n = 1.63) and ethanol (n = 1.36). The fraction of each mixture component was selected to match the refractive index of the soda lime (n = 1.52) or the borosilicate (n = 1.56) glass beads. Fig. S1(a–c) (ESI†) shows representative confocal micrographs of beds with bead diameters of 5.4 μm, 10 μm, and 30 μm. We acquired 25–30 two-dimensional images at different locations in the beds. The images were then binarized to identify pores and particles. First, 5000 points were randomly chosen inside the pore space. Next, we created eight vectors at each point that were equally spaced in the angular direction and expanded the vectors in both negative and positive directions until they met the surface of the particles. At a given point, we then summed the values of the negative and positive vectors for each angular direction to calculate the average chord length there. Similarly, the minimum chord length was also calculated from the minimum value of chord length at each point among all the angular directions.[40] Fig. S1(d–f) (ESI†) shows the probability distribution functions (PDFs) of the chord length and the minimum chord length in porous media with bead diameters of 5.4 μm, 10 μm, and 30 μm. The distributions are best fit to a gamma function, $G(l_{chord}) = \frac{1}{b^a \Gamma(a)} l_{chord}^{a-1} \exp\left(-\frac{l_{chord}}{b}\right)$, where l_{chord} is the chord length, $G(l_{chord})$ is the probability distribution of the chord length, and a and b are fitting parameters.

Table 1 Porosity, pore size (average chord length), and confinement length (average minimum chord length) of the porous media with bead diameters of 5.4 μm, 10 μm, and 30 μm

Bead diameter (μm)	Porosity	$\langle l_{chord} \rangle$ (μm)	$\langle l_{chord,min} \rangle$ (μm)
5.4	0.36 ± 0.07	4.4 ± 0.8	2.7 ± 0.7
10	0.34 ± 0.06	6.4 ± 1.1	3.7 ± 1.0
30	0.34 ± 0.06	14.7 ± 2.6	8.0 ± 1.1

Table 1 shows the porosity ϕ, pore size (average chord length) $d_{pore} = \langle l_{chord} \rangle$, and confinement length (average minimum chord length) $l_c = \langle l_{chord,min} \rangle$ of the porous media with different bead diameters.

Rheology of hydrolyzed polyacrylamide solution

The viscosity of the HPAM solution was measured using an ARES rheometer equipped with a double Couette geometry (inner diameter of 32 mm and outer diameter of 34 mm). We measured the (linear) elastic ($G'(\omega)$) and loss ($G''(\omega)$) moduli of the HPAM solution as a function of frequency (ω = 0.01–100 rad s^{-1}) in the linear viscoelastic regime and calculated the complex viscosity $\eta^*(\omega) = [G'^2(\omega) + G''^2(\omega)]^{1/2}/\omega$ as a function of angular frequency. We also measured the (nonlinear) viscosity as a function of shear rate, $\eta(\dot{\gamma})$. The shear-thinning behavior of the viscosity is modeled using a power law function, $\eta^* = k\omega^{n-1}$, where k = 0.62 and n = 0.36 are fitting parameters. The polymer relaxation time, $\lambda \approx 15$ s, is extracted from the bulk rheology at low frequencies where the viscosity approaches a constant value.

Conflict of interest

The authors declare no conflict of interest.

Acknowledgements

R. K. acknowledges funding from ExxonMobil Company. J. C. C. acknowledges funding from NSF (CBET-1438204) and the Welch Foundation (E-1869).

References

1 R. Tang, C. S. Kim, D. J. Solfiell, S. Rana, R. Mout, E. M. Velázquez-Delgado, A. Chompoosor, Y. Jeong, B. Yan, Z.-J. Zhu, C. Kim, J. A. Hardy and V. M. Rotello, *ACS Nano*, 2013, **7**, 6667–6673.
2 M.-H. Hsiao, Q. Mu, Z. R. Stephen, C. Fang and M. Zhang, *ACS Macro Lett.*, 2015, **4**, 403–407.
3 H. Ehtesabi, M. M. Ahadian and V. Taghikhani, *Energy Fuels*, 2015, **29**, 423–430.
4 J. F. Moll, P. Akcora, A. Rungta, S. Gong, R. H. Colby, B. C. Benicewicz and S. K. Kumar, *Macromolecules*, 2011, **44**, 7473–7477.
5 J. Moll, S. K. Kumar, F. Snijkers, D. Vlassopoulos, A. Rungta, B. C. Benicewicz, E. Gomez, J. Ilavsky and R. H. Colby, *ACS Macro Lett.*, 2013, **2**, 1051–1055.
6 D. Koch and J. F. Brady, *J. Fluid Mech.*, 1985, **154**, 399–427.

7 U. M. Scheven, *Phys. Rev. Lett.*, 2013, **110**, 214504.
8 S. Kenney, K. Poper, G. Chapagain and G. F. Christopher, *Rheol. Acta*, 2013, **52**, 485–497.
9 G. R. Moss and J. P. Rothstein, *J. Non-Newtonian Fluid Mech.*, 2010, **165**, 1–13.
10 M. Vasudevan, E. Buse, D. Lu, H. Krishna, R. Kalyanaraman, A. Q. Shen, B. Khomami and R. Sureshkumar, *Nat. Mater.*, 2010, **9**, 436–441.
11 L. Campo-Deaño, F. J. Galindo-Rosales, F. T. Pinho, M. A. Alves and M. S. N. Oliveira, *Soft Matter*, 2012, **8**, 6445–6453.
12 T. Burghelea, E. Segre, I. Bar-Joseph, A. Groisman and V. Steinberg, *Phys. Rev. E: Stat., Nonlinear, Soft Matter Phys.*, 2004, **69**, 066305.
13 A. Groisman, M. Enzelberger and S. R. Quake, *Science*, 2003, **300**, 955–958.
14 C. Scholz, F. Wirner, J. R. Gomez-Solano and C. Bechinger, *EPL*, 2014, **107**, 54003.
15 S. S. Datta, H. Chiang, T. S. Ramakrishnan and D. A. Weitz, *Phys. Rev. Lett.*, 2013, **111**, 064501.
16 U. M. Scheven, R. Harris and M. L. Johns, *Phys. Rev. Lett.*, 2007, **99**, 054502.
17 J. Frechette and G. Drazer, *J. Fluid Mech.*, 2009, **627**, 379–401.
18 L. R. Huang, E. C. Cox, R. H. Austin and J. C. Sturm, *Science*, 2004, **304**, 987–990.
19 K. He, S. T. Retterer, B. R. Srijanto, J. C. Conrad and R. Krishnamoorti, *ACS Nano*, 2014, **8**, 4221–4227.
20 T. Sochi, *Polymer*, 2010, **51**, 5007–5023.
21 S. P. Sullivan, L. F. Gladden and M. L. Johns, *J. Non-Newtonian Fluid Mech.*, 2006, **133**, 91–98.
22 J. Bleyer and P. Coussot, *Phys. Rev. E: Stat., Nonlinear, Soft Matter Phys.*, 2014, **89**, 063018.
23 T. Chevalier, S. Rodts, X. Chateau, C. Chevalier and P. Coussot, *Phys. Rev. E: Stat., Nonlinear, Soft Matter Phys.*, 2014, **89**, 023002.
24 R. H. Colby, *Rheol. Acta*, 2010, **49**, 425–442.
25 F. Babaye Khorasani, R. Poling-Skutvik, R. Krishnamoorti and J. C. Conrad, *Macromolecules*, 2014, **47**, 5328–5333.
26 W. P. Cox and E. H. Merz, *J. Polym. Sci.*, 1958, **28**, 619–622.
27 J. C. Crocker and D. G. Grier, *J. Colloid Interface Sci.*, 1996, **179**, 298–310.
28 B. Bijeljic, A. Raeini, P. Mostaghimi and M. Blunt, *Phys. Rev. E: Stat., Nonlinear, Soft Matter Phys.*, 2013, **87**, 013011.
29 B. Bijeljic, P. Mostaghimi and M. J. Blunt, *Phys. Rev. Lett.*, 2011, **107**, 204502.
30 L.-H. Cai, S. Panyukov and M. Rubinstein, *Macromolecules*, 2011, **44**, 7853–7863.
31 R. S. Maier, D. M. Kroll, R. S. Bernard, S. E. Howington, J. F. Peters and H. T. Davis, *Phys. Fluids*, 2000, **12**, 2065–2079.
32 D. Kandhai, D. Hlushkou, A. G. Hoekstra, P. M. A. Sloot, H. Van As and U. Tallarek, *Phys. Rev. Lett.*, 2002, **88**, 234501.
33 B. Bijeljic and M. Blunt, *Water Resour. Res.*, 2007, **43**, W12S11.
34 H. Bodiguel, J. Beaumont, A. Machado, L. Martinie, H. Kellay and A. Colin, *Phys. Rev. Lett.*, 2015, **114**, 028302.
35 R. Medina, J. E. Elkhoury, J. P. Morris, R. Prioul, J. Desroches and R. L. Detwiler, *Geofluids*, 2015, **15**, 24–36.
36 Y. Ruan, L. Gao, D. Yao, K. Zhang, B. Zhang, Y. Chen and C.-Y. Liu, *ACS Macro Lett.*, 2015, **4**, 1067–1071.
37 S. Fekete, D. Guillarme, P. Sandra and K. Sandra, *Anal. Chem.*, 2016, **88**, 480–507.
38 H. N. Chia and B. M. Wu, *J. Biol. Eng.*, 2015, **9**, 4.
39 S. K. Kumar and R. Krishnamoorti, *Annu. Rev. Chem. Biomol. Eng.*, 2010, **1**, 37–58.
40 D. Stoeckel, C. Kübel, K. Hormann, A. Höltzel, B. M. Smarsly and U. Tallarek, *Langmuir*, 2014, **30**, 9022–9027.